H-*T* phase diagram of rare-earth–transition-metal alloys in the vicinity of the compensation point

M. D. Davydova,[1,2] K. A. Zvezdin,[1,2] J. Becker,[3] A. V. Kimel,[3] and A. K. Zvezdin[2,4,*]

[1]*Moscow Institute of Physics and Technology (State University), 141700 Dolgoprudny, Russian Federation*
[2]*Prokhorov General Physics Institute of the Russian Academy of Sciences, 119991 Moscow, Russian Federation*
[3]*Institute for Molecules and Materials, Radboud University, Nijmegen 6525 AJ, Netherlands*
[4]*Lebedev Physical Institute of the Russian Academy of Sciences, 119333 Moscow, Russian Federation*

Anomalous hysteresis loops of ferrimagnetic amorphous alloys in high magnetic field in the vicinity of the compensation temperature have so far been explained by sample inhomogeneities. We obtain the *H*-*T* magnetic phase diagram for the ferrimagnetic GdFeCo alloy using a two-sublattice model in the paramagnetic rare-earth ion approximation and taking into account rare-earth (Gd) magnetic anisotropy. It is shown that if the magnetic anisotropy of the f sublattice is larger than that of the d sublattice, the tricritical point can be at higher temperature than the compensation point. The obtained phase diagram explains the observed anomalous hysteresis loops as a result of high-field magnetic phase transition, the order of which changes with temperature. It also implies that in the vicinity of the magnetic compensation point the shape of magnetic hysteresis loop strongly depends on temperature.

I. INTRODUCTION

Rare-earth amorphous alloys and intermetallics are a large class of magnetic materials allowing us to change their magnetic properties in a wide range through a subtle change in the composition, temperature, or application of magnetic field [1–5]. The materials have already found applications as hard magnets and recording media, and they still offer a rich playground in the areas of spintronics [6], magnonics [7], and ultrafast magnetism [8–17].

GdFeCo is a particular example of such an amorphous alloy. It is a $3d$-$4f$ ferrimagnet with compensation temperature [18], at which the magnetizations of the two sublattices become equal. At temperatures lower than the compensation temperature, the magnetization of the rare-earth (Gd) sublattice M_f is larger than that of the transition metal (Fe) M_d ($M_f - M_d > 0$), whereas at higher temperatures $M_f - M_d < 0$. Many studies of GdFeCo, GdFe, and GdCo compounds as well as magnets with different rare-earth ions in high magnetic field revealed triple hysteresis loops in the vicinity of the magnetization compensation point [19–23]. The observed triple loops are clearly different from the hysteresis loop normally expected for a single thin film, where one would not expect a sudden decrease in magnetization in the strong applied magnetic field. However, hysteresis loops of this form are typical for multilayered structures. To emphasize the difference, we will refer to the loops in single-layer structures as anomalous. These loops are strongly dependent on temperature. Earlier similar behavior was explained by sample inhomogeneities [23] or strong exchange bias between surface and bulk layers that have different stoichiometric compositions of the alloy;

in particular, this has led to the estimation of the strongest reported exchange bias field of several teslas [24]. However, to date no theoretical model has been proposed that would allow us to calculate magnetization curves that would explain experimental data. In this paper, we use a model for a homogeneous two-sublattice ferrimagnet film and suggest an alternative explanation for the observed anomalous hysteresis loops.

Figure 1 shows the results of high-magnetic-field measurements of the magneto-optical Kerr effect in GdFeCo [22]. The composition of the alloy with 24% Gd, 66.5% Fe, and 9.5% Co resulted in the compensation temperature $T_{comp} = 283$ K. The field was applied at the normal to the sample, which is also the easy magnetization axis. The measurements were done at the probe wavelength of 630 nm in the polar Kerr geometry. In this case the probe is predominantly sensitive to the magnetization of the Fe sublattice. Therefore, the obtained hysteresis loops reveal the field dependence of the orientation of the Fe magnetization.

It is seen that upon an increase of the field, first, a minor hysteresis loop shows up, which corresponds to the magnetization reversal. A further increase of the field does not change the orientation of the magnetization until a critical field is reached. This field launches a spin-flop transition, which is seen as a decrease of the magneto-optical signal. At this field the magnetizations of the sublattices turn from the normal of the sample, get canted, and form a noncollinear state. The character of the spin-flop transition changes with temperature. Below the magnetic compensation temperature the spin-flop transition occurs gradually (see loops for 260 and 277 K in Fig. 1). Just above the compensation point at the spin-flop field one observes an abrupt change in the magnetic structure (see loops for 289 and 291 K in Fig. 1). Upon a further increase of the sample temperature the transition is seen as gradual again (see loop at 321 K in Fig. 1). Abrupt and gradual
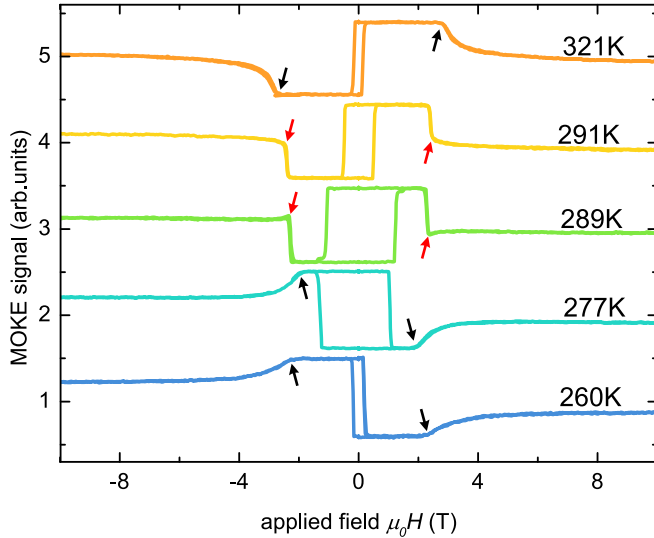
*zvezdin.ak@phystech.edu

FIG. 1. Static magneto-optic Kerr effect in a GdFeCo sample measured at 630-nm probe wavelength at different temperatures from 260 to 321 K. A paramagnetic background was subtracted from the measurements. The compensation temperature is 283 K [22]. Black and red arrows indicate second- and first-order transitions, respectively.

changes in magnetization induced by external magnetic field are characteristic features of first- and second-order phase transitions, respectively. Hence, these measurements imply that the order of the phase transition changes from second to first and back to second upon a temperature increase across the compensation point. Such a temperature-dependent order of the spin-flop transition has not been described for GdFeCo in the literature before.

Note that, although phase diagrams for $3d$-$4f$ ferrimagnets were first obtained theoretically almost 50 years ago [25,26] and supported by numerous experiments (see [27] and references therein), in the studies performed so far the anisotropy of the transition-metal sublattice was taken to be larger than that of the rare-earth sublattice. The existing results for the magnetic phase diagrams fail to explain the anomalous hysteresis loops observed experimentally [22–24]. Unusual behavior of the critical fields in rare-earth intermetallics in the case of prevailing anisotropy of the rare-earth sublattice was recently investigated by some of the authors theoretically for HoFe$_x$Al$_{12-x}$ [28,29]. Here we show that if the rare-earth anisotropy is larger than that of the transition metal, the tricritical point on the phase diagram lies at higher temperatures with respect to the compensation point. As a result, the observed hysteresis loops can be explained in terms of intrinsic first- and second-order phase transitions in the intermetallic samples.

II. MAGNETIC PHASE DIAGRAM

To obtain the H-T phase diagram, we derive the thermodynamic potential for a two-sublattice ferrimagnet in the paramagnetic rare-earth ion approximation [25–27]. We start with the Hamiltonian for a system of f and d ions in an external magnetic field in the form [30]

$$\mathcal{H} = \mathcal{H}_f + \mathcal{H}_{f-d} + \mathcal{H}_d, \tag{1}$$

where

$$\mathcal{H}_d = \mathcal{H}_{cr}^d - \sum_{i_1, i_2 \in d} \mathcal{J}_{i_1 i_2}^d \boldsymbol{S}_{i_1} \boldsymbol{S}_{i_2} + \left| g_J^d \right| \mu_B \boldsymbol{H} \sum_{i \in d} \boldsymbol{J}_i,$$

$$\mathcal{H}_{f-d} = - \sum_{i_1 \in f, i_2 \in d} \mathcal{J}_{i_1 i_2}^{f-d} \boldsymbol{S}_{i_1} \boldsymbol{S}_{i_2},$$

$$\mathcal{H}_f = \mathcal{H}_{cr}^f + \left| g_J^f \right| \mu_B \boldsymbol{H} \sum_{i \in f} \boldsymbol{J}_i. \tag{2}$$

In the one-sublattice Hamiltonian $\mathcal{H}_d$ for the d sublattice the first term represents the crystal field Hamiltonian (see the Appendix), the second term is the intrasublattice exchange interaction, and the last term is the Zeeman energy in the external magnetic field $\boldsymbol{H}$. The second component, $\boldsymbol{H}_{f-d}$, of the total Hamiltonian is the intrasublattice exchange interaction. The f-sublattice Hamiltonian $\mathcal{H}_d$ consists of crystal field and Zeeman energy. We neglect the exchange within the f sublattice because its magnitude is several orders smaller than f-d exchange [30]. The summation is performed over the ions belonging to f and d sublattices, $\boldsymbol{J}_i = \boldsymbol{L}_i + \boldsymbol{S}_i$ is the total angular momentum of an operator for the ith ion, and $\mathcal{J}^d$ and $\mathcal{J}^{f-d}$ are the matrices of the exchange interaction within one sublattice and between sublattices, respectively. In the following, we assume the g factors for rare-earth and transition metal s ions are $g \equiv |g_J^f| \approx |g_J^d| \approx 2$.

Using the procedure described in the Appendix, we derive the thermodynamic potential of the nonequilibrium state (effective free energy) where the parameter is the orientation of the d-sublattice magnetization vector $\boldsymbol{M}_d$. The value of this magnetization is assumed to be saturated due to the large d-d exchange with a corresponding exchange field of the order of 10^6–10^7 Oe. We also assume that the magnetization of the f sublattice is defined by the effective magnetic field acting on it, $\boldsymbol{H}_{\text{eff}} = \boldsymbol{H} - \lambda \boldsymbol{M}_d$, where λ is the f–d exchange coupling constant (see the Appendix). Finally, we arrive at the thermodynamic potential in the form given by Eq. (3). Finally, we obtain

$$\Phi = -\boldsymbol{M}_d \cdot \boldsymbol{H} - \int_0^{H_{\text{eff}}} g J B_J \left(\frac{g J \mu_B h}{kT} \right) dh + K_f \sin^2 \theta_f$$
$$+ K_d \sin^2 \theta_d, \tag{3}$$

where $B_J(x)$ is the Brillouin function, $J = 7/2$ is the ground state total angular momentum of the Gd ion, and K_f and K_d denote the uniaxial magnetic anisotropy constants for the two sublattices, which are assumed to have different values. In our spherical coordinate system, the polar axis lies in the direction of the easy magnetization axis, and the angles θ_f and θ_d are the polar angles for magnetizations of rare-earth and transition-metal sublattices, respectively.

When the magnetic field $\boldsymbol{H}$ is applied along the easy axis, the effective free energy may be represented as a function of
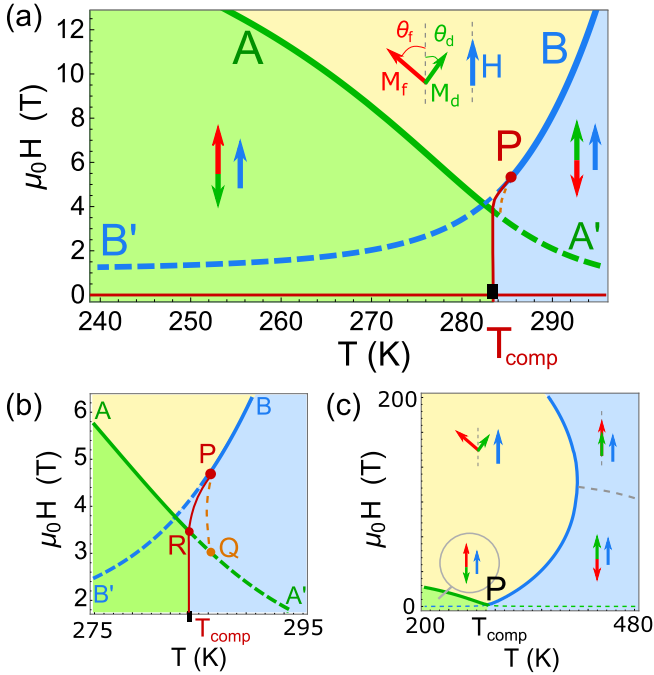
FIG. 2. (a) The *H-T* phase diagram near the compensation point T_{comp} for GdFeCo in magnetic field directed along the easy magnetization axis. The dashed lines are the stability loss lines for the corresponding phases; solid lines correspond to the lines of phase transitions. (b) The magnified area of the *H-T* phase diagram near the tricritical point *P*. The line *PQ* corresponds to the stability loss of the noncollinear phase. (c) The qualitative zoomed-out *H-T* phase diagram up to magnetic fields of the order of 200 T.
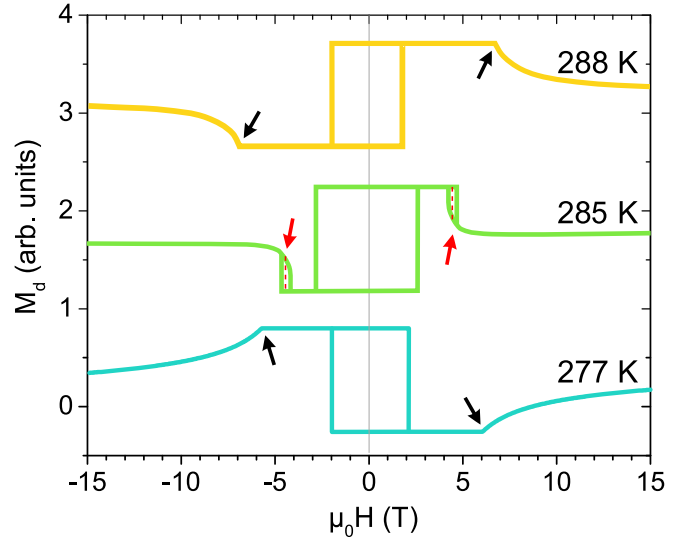

FIG. 3. Dependence of the component of the *d*-sublattice magnetization along the easy-axis direction on the magnetic field at different temperatures. Black and red arrows indicate second- and first-order transition points, respectively.

just one order parameter θ_d:

$$\Phi = -M_d H \cos\theta_d - \int_0^{H_{\text{eff}}(\theta_d)} gJB_J\left(\frac{gJ\mu_B h}{kT}\right)dh$$

$$+ K_f\left(\frac{\lambda M_d \sin\theta_d}{H_{\text{eff}}(\theta_d)}\right)^2 + K_d \sin^2\theta_d, \qquad (4)$$

where $H_{\text{eff}}(\theta_d) = \sqrt{H^2 + \lambda^2 M_d^2 - 2H\lambda M_d \cos\theta_d}$.

Using the expression for the thermodynamic potential (4) and the method described in Ref. [27], we numerically calculate the magnetic phase diagram in the coordinates "*H-T*" (Fig. 2) and calculate the magnetization curves shown in Fig. 3. The ground states of the system are found by minimization of the thermodynamic potential (4) with regard to the order parameter θ_d. At the minima one finds $\frac{\partial\Phi}{\partial\theta_d} = 0$ and $\frac{\partial^2\Phi}{\partial\theta_d^2} > 0$. The lines of stability loss, where $\frac{\partial^2\Phi}{\partial\theta_d^2} = 0$, are found for each phase. In terms of Landau theory of the phase transitions, if the thermodynamic potential is written in terms of Taylor series with respect to the order parameter $\Phi = a(H,T)\theta_d^2 + \frac{1}{2}b(H,T)\theta_d^4 + c(H,T)\theta_d^6 + \cdots$, the second-order phase transition is observed when $a(H,T) = 0$ and $b(H,T)$ is positive. If $a(H,T) > 0$, $c(H,T) > 0$, but $b(H,T) < 0$, the system undergoes the first-order phase transition.

Near the first-order phase transition two possible stationary states coexist, corresponding to one local (metastable) and one global (stable) minimum of the thermodynamic potential.

For the numerical calculations, we used the following set of parameters: $T_{\text{comp}} = 283$ K, $T_C = 500$ K, $M_f(0) = 7\ \mu_B/\text{f.u.}$, $M_d(0) = 6.5\ \mu_B/\text{f.u.}$, and the exchange constant $\lambda = 22\ \text{T}/\mu_B$. To the best of our knowledge, no experimental data for the strength of the magnetic anisotropy of the rare-earth sublattice are available for the GdFeCo alloy. Nevertheless, until now it has been believed that the magnetic anisotropy of the Gd sublattice is smaller than that of the iron sublattice. Here we show that by taking $K_f \approx 0.6$ K/f.u. and neglecting the *d*-sublattice anisotropy one obtains a qualitative agreement of the calculated magnetic phase diagram with the experimental data from the recent study [22].

For analytical investigation of the phase diagram, we describe the two-sublattice ferrimagnet in terms of the antiferromagnetic vector $\boldsymbol{L} = \boldsymbol{M}_f - \boldsymbol{M}_d$ and the net magnetization $\boldsymbol{M} = \boldsymbol{M}_f + \boldsymbol{M}_d$. Note that in the vicinity of the compensation point the difference between the sublattice magnetizations $|M_f - M_d| \ll L$ is small but not zero. These two vectors are parametrized using sets of angles θ, ε, φ, and β. The angles are defined so that

$$\theta_f = \theta - \varepsilon, \quad \theta_d = \pi - \theta - \varepsilon,$$
$$\varphi_f = \varphi - \beta, \quad \varphi_d = \pi + \varphi + \beta, \qquad (5)$$

where φ_f and φ_d are the azimuthal angles for magnetizations of rare-earth and transition-metal sublattices, respectively. In the chosen coordinate system the azimuthal axis lies in plane perpendicular to the easy axis. In this case the antiferromagnetic vector may be naturally defined as $\boldsymbol{L} = (L\sin\theta\cos\varphi, L\sin\theta\sin\varphi, L\cos\theta)$. In the vicinity of the second-order phase transition the expansion of the thermodynamic potential (3) may be performed in the series of angles θ, ε, φ, and β, which can be seen as the order parameters. Using the expansion, we obtain analytical expressions that describe the behavior of the order parameters in different phases in the vicinity of the compensation temperature.

In the collinear phase to the left of the compensation point [green area in Fig. 2(a)] the parameter θ is equal to zero. To the right of the compensation temperature a collinear phase with $\theta = \pi$ is the stable phase [blue area in Fig. 2(a)]. The noncollinear phase, which is shown in Fig. 2(a) by a yellow area, can be described by analytical expression

$$\cos\theta \approx -\frac{\chi\left(H^2 - H_1^2\right)}{6\chi H \Delta H_A} \pm \frac{\sqrt{\chi^2\left(H^2 - H_1^2\right)^2 + 12\chi H^2 \Delta H_A[(M_f - M_d) + \chi \Delta H_A]}}{6\chi H \Delta H_A}, \tag{6}$$

where $\chi = (M_f + M_d)^2/(2M_d M_f \lambda)$, $H_1^2 = 2\frac{K_d + K_f}{\chi}$, and $\Delta H_A = 2\frac{K_f - K_d}{M_f + M_d}$. If the condition $\Delta H_A > 0$ is satisfied, the first-order transition between the noncollinear and the collinear phases $\theta = \pi$ will occur at temperatures higher than the compensation point, which follows from expression (6).

III. RESULTS AND DISCUSSION

Three different phases are present in the magnetic phase diagram. For convenience, we label the phases by the orientation of antiferromagnetic vector $\boldsymbol{L} = \boldsymbol{M}_f - \boldsymbol{M}_d$ in these phases and also schematically show the magnetization orientations in each phase in Figs. 2(a) and 2(c). The phases are the low-temperature collinear phase $\theta = 0$ (green area), the high-temperature collinear phase $\theta = \pi$ (blue area), and the noncollinear (angular) phase $\theta = \theta(H, T)$ (yellow area), which is described by Eq. (6). The collinear phase $\theta = 0$ exists below line AA', whereas the collinear phase $\theta = \pi$ exists below line BB'. These lines are the stability loss lines for the corresponding phases. The area of the angular phase is limited from below by the curve $AQPB$. The zoomed-in area of the phase diagram around point P is shown in Fig. 2(b), and the zoomed-out phase diagram is shown in Fig. 2(c) along with schematically drawn directions of the sublattice magnetizations in each phase. At the dashed gray line in Fig. 2(c) the condition $H_{\text{eff}}(T) = 0$ is fulfilled.

There are several first- and second-order phase transitions in the vicinity of the magnetization compensation temperature T_{comp}. The second-order phase transitions are denoted by the solid lines AR and PB and are characterized by a continuous change of the order parameter across the line. The dashed lines in Fig. 2 are the lines of the stability loss and denote the theoretical temperature-dependent boundaries for the field hysteresis around the first-order phase transition at $H = 0$. The solid line between T_{comp} and point P corresponds to another and less trivial first-order phase transition. The magnified area of the magnetic phase diagram in the vicinity of point P is shown in Fig. 2(b). The line $T_{\text{comp}}R$ corresponds to the line at which the two collinear phases ($\theta = 0$ and $\theta = \pi$) have equal thermodynamic potentials $\Phi(0) = \Phi(\pi)$ and represents the first-order magnetic phase transition. Both phases coexist to the left and to the right of $T_{\text{comp}}R$. Above AR there is no minimum of the thermodynamic potential for the collinear phase $\theta = 0$ anymore, and the spins turn continuously into the noncollinear phase. At line RP the first-order phase transition continues, but now it is the transition between the angular phase and the collinear $\theta = \pi$ phase. At point P the order of the transition changes from first to second. According to the conventional classification, this is a tricritical point [31],

in the vicinity of which many physical quantities, such as heat capacity and magnetic susceptibility, experience anomalous behavior.

The first-order phase transition across line $T_{\text{comp}}P$ and the tricritical point in rare-earth ferrimagnets with similar properties were reported earlier [25,26]. However, in the previous studies it was claimed that the temperature corresponding to the tricritical point is smaller than the magnetization compensation temperature, $T_P < T_{\text{comp}}$. The anomalous temperature-dependent hysteresis loops in the vicinity of the compensation point of ferrimagnets observed earlier, and it was believed that the observed hysteresis loops are due to inhomogeneities. The relation between this previously overlooked first-order phase transition and the observed hysteresis behavior is as follows. Applying an external magnetic field and measuring the magnetization behavior, one expects to observe a minor hysteresis loop corresponding to the first-order phase transition between two collinear phases, $\theta = 0$ and $\theta = \pi$. The coercive field of this minor hysteresis loop increases upon approaching the compensation temperature. In the temperature range between the compensation and tricritical points ($T_{\text{comp}} < T < T_P$) upon an increase of the external magnetic field the compound undergoes not one but two first-order phase transitions. The first one results in a hysteresis loop around $H = 0$, as explained above. The second is the spin-flop transition to the noncollinear phase, which will also result in hysteresis at higher magnetic fields. The size of the second jump of magnetization and its hysteresis will then decrease and, subsequently, vanish at the tricritical point.

Figure 3 shows the calculated magnetic field dependencies of the normal component of the d-sublattice magnetization at various temperatures in the vicinity of the compensation point. One can see a remarkable qualitative agreement of the calculations with anomalous temperature-dependent hysteresis loops previously observed in rare-earth transition-metal alloys experimentally. Hence, here we have suggested an alternative explanation of the anomalous hysteresis loops without relying on inhomogeneities and large exchange-bias field. The observed hysteresis loops can be seen as an intrinsic property and explained in terms of first- and second-order phase transitions in the compound.

In the past decade the spin dynamics of rare-earth transition-metal alloys has attracted intense research interest due to the unique capability of these materials to reverse their magnetization at record-breaking speed under the action of subpicosecond laser pulses [8]. In the research aiming to understand the mechanisms of the ultrafast laser-induced magnetization reversal computational methods have been playing a decisive role [9,11,13,32–34]. It is clear that the value of the magnetic anisotropy of the rare-earth sublattice in

ferrimagnets is an important input parameter which may greatly influence the outcome of such simulations. In GdFeCo, the rare-earth anisotropy constant may be expected to be larger than that of iron because the strength of the spin-orbit coupling depends on the nucleus charge Z very close to the Z^4 law (for more accurate evaluations, see Refs. [35,36]). Taking into account excited multiplets with nonzero orbital angular momentum L, the large single-ion anisotropy can be explained as a result of the spin-orbit coupling and the crystal field. More specifically, the large rare-earth anisotropic contribution can be calculated from microscopic theory by taking into account the local crystal field of a single rare-earth ion environment and spin-orbit coupling simultaneously: $\hat{V} = \sum_i \lambda_{SO} \hat{l}_i \hat{s}_i + \sum_i \sum_{k,q} B_k^q \hat{C}_q^k(l_i)$, where λ_{SO} is the spin-orbit coupling constant, index i spans f electrons of the Gd^{3+} ion, B_k^q are the crystal field parameters, and $\hat{C}_q^k(l_i)$ are the irreducible tensor operators. In perturbation theory of the third order and by taking into account states from both ground ^8S and excited ^6P terms, one obtains the spin Hamiltonian with a contribution of the form $D[S_z^2 - \frac{1}{3}S(S+1)]$ [37–39]. The existing estimations of D from both theory and experiment [40] are of the order of 10^{-2}–10^{-1} cm^{-1} per ion. Such a value corresponds to the large gadolinium anisotropy constant K_f used in our calculations.

Moreover, it is expected that in compounds with rare-earth ions with nonzero orbital momentum in the ground state (Tb, Dy, Sm), the effect of the rare-earth magnetic anisotropy will be even more pronounced than in the case of Gd. For instance, in the simulations of TbCo [33] in order to mimic the experimentally observed dependence of magnetic anisotropy on the concentration of Tb, it was necessary to set a 10 times larger anisotropy for the Tb sublattice compared to the one of Co. Our work provides an approach for experimental verification of element-specific magnetic anisotropies in rare-earth transition-metal ferrimagnets.

IV. CONCLUSION

In conclusion, we investigated the *H-T* phase diagram for a rare-earth transition-metal ferrimagnet in the case of magnetic field directed along the easy magnetization axis. We showed that if the rare-earth anisotropy is larger than that of the d sublattice, the spin-flop transition from the collinear to noncollinear phase is either the first- or second-order phase transition. Just above the compensation temperature the phase transition is of the first order. Starting from the tricritical point P, at higher temperatures the spin flop becomes a phase transition of the second order. Such a temperature-dependent order of the transition from collinear to noncollinear spin phase allows us to explain anomalous hysteresis loops in rare-earth transition-metal alloys without involving the exchange bias between the surface and the bulk. Hence, we suggest that such hysteresis loops are an intrinsic property of alloys of the GdFeCo type, which have become model materials in spintronics [41], magnonics [15,42], and ultrafast magnetism [14,43–45]. Note that at the tricritical point many response functions (heat capacity, magnetic susceptibility, etc.) experience anomalous behavior, which opens totally new opportunities for fundamental and applied research of the alloys.

APPENDIX: DERIVATION OF THE THERMODYNAMIC POTENTIAL

We start from a more general form of the Hamiltonian introduced in Eq. (1) that includes exchange interaction within the f sublattice. This term can often be neglected due to its smallness [30]. First, we restrict ourselves to a ground-state term and use the Wigner-Eckart theorem to express the spin operators S_i through total mechanical momentum J_i. We obtain the components of the total Hamiltonian:

$$\mathcal{H}_{f,d} = \mathcal{H}_{cr}^{f,d} - \frac{1}{2}\left(g_J^{f,d}\right)^2 \mu_B^2 \sum_{i_1, i_2 \in f,d} J_{i_1} T_{i_1 i_2}^{f,d} J_{i_2}$$
$$+ \left|g_J^{f,d}\right| \mu_B H \sum_{i \in f,d} J_i,$$
$$\mathcal{H}_{f-d} = -g_J^d g_J^f \mu_B^2 \sum_{i_1 \in f, i_2 \in d} J_{i_1} T_{i_1 i_2}^{f-d} J_{i_2}, \qquad \text{(A1)}$$

where the exchange matrices $T_{d,f}$ and T_{f-d} are linearly proportional to those of $\mathcal{J}^{d,f}$ and $\mathcal{J}^{f-d}$. We introduce the effective free energy (the thermodynamic potential of the nonequilibrium state; see Ref. [30]) that is a function of both magnetic field and magnetizations $M_{f,d}$:

$$\Phi = F + h_f M_f + h_d M_d, \qquad \text{(A2)}$$

where

$$F = -T \ln \text{Tr}\{\exp -(\beta[\mathcal{H} - h_f \hat{M}_f - h_d \hat{M}_d])\} \qquad \text{(A3)}$$

is the thermodynamic free energy, $\beta = 1/(kT)$, and the total sublattice magnetization operators are $\hat{M}_{f,d} = g\mu_B \sum_{i \in f,d} J_i$. The equations for the sublattice magnetizations $M_{f,d} = -\frac{\partial F}{\partial h_{f,d}}$ are viewed as the conditions defining the values of Lagrange multipliers h_f and h_d. In the derivation, we take the trace over the ground-state terms, whereas tracing for the excited states may account for a large rare-earth ion anisotropy. This question was discussed above in [30].

Using the fact that the intersublattice exchange energy is two to three orders of magnitude smaller than the exchange within the d subsystem, we assume the f-d homogeneous Heisenberg exchange is equal to

$$\mathcal{H}_{f-d} = \widetilde{\mathcal{H}}_{f-d} = -\frac{1}{N_d} g\mu_B \sum_{i_1 \in f, i_2 \in d} J_{i_1} T_{i_1 i_2}^{f-d} M_d \qquad \text{(A4)}$$

and substitute the total magnetic moment operator d subsystem with its average value M_d, which might be found from a more refined theory or experiment [30]. From this equation, the f-d exchange coupling constant λ can be determined.

In our approximation, the absolute value of the magnetization M_d is saturated by the d exchange, and only its direction varies. The matrix elements of the crystal field Hamiltonian are small in comparison to both exchanges; thus, we can treat

it perturbatively. We also neglect the f-f exchange. We obtain

$$\Phi = -\boldsymbol{M}_d \cdot (\boldsymbol{H} - \boldsymbol{h}_d) + \langle \mathcal{H}_{cr}^d \rangle$$
$$- T \ln \mathrm{Tr}_f \{ \exp(\beta[\mathcal{H}_f + \widetilde{\mathcal{H}}_{f-d} - \boldsymbol{h}_f \hat{\boldsymbol{M}}_f]) \} + \boldsymbol{h}_f \boldsymbol{M}_f,$$
(A5)

where Tr_f denotes the trace over the f-subsystem ground-state term states. This is a quite general result that allows for a high-accuracy treatment of f-d magnets. For subsequent consideration we simplify this expression further. For a GdFeCo-like alloy the single-ion crystal field for both sublattices may be represented by its first term of expansion $(\mathcal{H}_{cr}^{f,d})_i = (A_0^2)_i \sum_j C_2^0(\boldsymbol{l}_j)$, where C_m^n are the Steven's operators [46] and $\boldsymbol{l}_j$ is the angular momentum of the jth electron belonging to the ith ion. According to Wigner-Eckart theorem, if we restrain our consideration to the ground-state term with given J, the result can be represented as a function of the total angular momentum of the ion: $(\mathcal{H}_{cr}^{f,d})_i = (B_0^2)_i Y_2^0(\boldsymbol{J}_i)$. When viewing the crystal field as a perturbation, we introduce the quantization axis along the external field and find the d-sublattice $\langle \mathcal{H}_{cr}^d \rangle = -4/3\sqrt{\pi/5}K_d Y_2^0(\boldsymbol{M}_d/M_d)$ [46], where Y_2^0 are the spherical harmonics and we have introduced the uniaxial magnetocrystalline anisotropy K_d.

Treating the crystal field acting on f ions as a perturbation (similar to d-crystal field), we also assume the magnetization $\boldsymbol{M}_f$ is aligned with the effective magnetic field acting on it and release the Lagrangian multiplier $\boldsymbol{h}_f$, obtaining the Brillouin function after tracing the third term in expression (A5): $M_f \approx g_{J_f} \mu_B N_f B_J(\frac{g_{J_f} \mu_B H_{\mathrm{eff}}}{kT})$, where $\boldsymbol{H}_{\mathrm{eff}} = \boldsymbol{H} - \lambda \boldsymbol{M}_d$ and the f-d exchange coupling constant is denoted as λ. The total angular momentum eigenvalue J_f for the ground-state term ^8S of Gd ions is equal to $7/2$. Finally, we arrive at the thermodynamic potential in the form given by Eq. (3).

---

[1] K. Buschow, Rep. Prog. Phys. **40**, 1179 (1977).

[2] J. Franse and R. Radwański, Handb. Magn. Mater. **7**, 307 (1993).

[3] K. P. Belov, A. K. Zvezdin, A. M. Kadomtseva, and R. Levitin, Sov. Phys. Usp. **19**, 574 (1976).

[4] N. Duc, D. K. Anh, and P. Brommer, Physica B (Amsterdam, Neth.) **319**, 1 (2002).

[5] V. Sechovský, L. Havela, K. Prokeš, H. Nakotte, F. De Boer, and E. Brück, J. Appl. Phys. **76**, 6913 (1994).

[6] I. Žutić, J. Fabian, and S. Das Sarma, Rev. Mod. Phys. **76**, 323 (2004).

[7] V. Kruglyak, S. Demokritov, and D. Grundler, J. Phys. D **43**, 264001 (2010).

[8] C. D. Stanciu, F. Hansteen, A. V. Kimel, A. Kirilyuk, A. Tsukamoto, A. Itoh, and T. Rasing, Phys. Rev. Lett. **99**, 047601 (2007).

[9] K. Vahaplar, A. M. Kalashnikova, A. V. Kimel, D. Hinzke, U. Nowak, R. Chantrell, A. Tsukamoto, A. Itoh, A. Kirilyuk, and T. Rasing, Phys. Rev. Lett. **103**, 117201 (2009).

[10] A. Moser, K. Takano, D. T. Margulies, M. Albrecht, Y. Sonobe, Y. Ikeda, S. Sun, and E. E. Fullerton, J. Phys. D **35**, R157 (2002).

[11] T. Ostler, J. Barker, R. Evans, R. Chantrell, U. Atxitia, O. Chubykalo-Fesenko, S. El Moussaoui, L. Le Guyader, E. Mengotti, L. Heyderman *et al.*, Nat. Commun. **3**, 666 (2012).

[12] A. R. Khorsand, M. Savoini, A. Kirilyuk, A. V. Kimel, A. Tsukamoto, A. Itoh, and T. Rasing, Phys. Rev. Lett. **108**, 127205 (2012).

[13] I. Radu, K. Vahaplar, C. Stamm, T. Kachel, N. Pontius, H. Dürr, T. Ostler, J. Barker, R. Evans, R. Chantrell *et al.*, Nature (London) **472**, 205 (2011).

[14] C. Graves, A. Reid, T. Wang, B. Wu, S. De Jong, K. Vahaplar, I. Radu, D. Bernstein, M. Messerschmidt, L. Müller *et al.*, Nat. Mater. **12**, 293 (2013).

[15] C. D. Stanciu, F. Hansteen, A. V. Kimel, A. Tsukamoto, A. Itoh, A. Kirilyuk, and T. Rasing, Phys. Rev. Lett. **98**, 207401 (2007).

[16] L. Le Guyader, S. El Moussaoui, M. Buzzi, R. Chopdekar, L. Heyderman, A. Tsukamoto, A. Itoh, A. Kirilyuk, T. Rasing, A. Kimel *et al.*, Appl. Phys. Lett. **101**, 022410 (2012).

[17] C. Xu, Z. Chen, D. Chen, S. Zhou, and T. Lai, Appl. Phys. Lett. **96**, 092514 (2010).

[18] R. C. Taylor and A. Gangulee, Phys. Rev. B **22**, 1320 (1980).

[19] S. Esho, Jpn. J. Appl. Phys. **15**, 93 (1976).

[20] T. Chen and R. Malmhäll, J. Magn. Magn. Mater. **35**, 269 (1983).

[21] K. Okamoto and N. Miura, Physica B (Amsterdam, Neth.) **155**, 259 (1989).

[22] J. Becker, A. Tsukamoto, A. Kirilyuk, J. C. Maan, T. Rasing, P. C. M. Christianen, and A. V. Kimel, Phys. Rev. Lett. **118**, 117203 (2017).

[23] M. Amatsu, S. Honda, and T. Kusuda, IEEE Trans. Magn. **13**, 1612 (1977).

[24] K. Chen, D. Lott, F. Radu, F. Choueikani, E. Otero, and P. Ohresser, Sci. Rep. **5**, 18377 (2015).

[25] B. F. Goransky and A. K. Zvezdin, ZhETF Pis. Red. **10**, 196 (1969) [JETP Lett. **10**, 124 (1969)].

[26] A. Zvezdin and V. Matveev, Sov. Phys. JETP **35**, 140 (1972).

[27] A. Zvezdin, Handb. Magn. Mater. **9**, 405 (1995).

[28] C. K. Sabdenov, M. Davydova, K. Zvezdin, A. Zvezdin, A. Andreev, D. Gorbunov, E. Tereshina, Y. Skourski, J. Šebek, and I. Tereshina, J. Alloys Compd. **708**, 1161 (2017).

[29] C. K. Sabdenov, M. Davydova, K. Zvezdin, D. Gorbunov, I. Tereshina, A. Andreev, and A. Zvezdin, J. Low Temp. Phys. **43**, 551 (2017).

[30] A. K. Zvezdin, V. M. Matveev, A. A. Mukhin, and A. I. Popov, *Rare Earth Ions in Magnetically Ordered Crystals* (Nauka, Moscow, 1985).

[31] I. D. Lawrie and S. Sarbach, Phase Trans. Crit. Phenom. **9**, 2 (1984).

[32] U. Atxitia, T. Ostler, J. Barker, R. F. L. Evans, R. W. Chantrell, and O. Chubykalo-Fesenko, Phys. Rev. B **87**, 224417 (2013).

[33] R. Moreno, T. A. Ostler, R. W. Chantrell, and O. Chubykalo-Fesenko, Phys. Rev. B **96**, 014409 (2017).

[34] R. Chimata, L. Isaeva, K. Kádas, A. Bergman, B. Sanyal, J. H. Mentink, M. I. Katsnelson, T. Rasing, A. Kirilyuk, A. Kimel, O. Eriksson, and M. Pereiro, Phys. Rev. B **92**, 094411 (2015).

[35] M. Blume and R. Watson, Proc. R. Soc. London, Ser. A **271**, 565 (1963).

[36] M. Blume, A. J. Freeman, and R. E. Watson, Phys. Rev. **134**, A320 (1964).

[37] J. Van Vleck and W. Penney, London, Edinburgh Dublin Philos. Mag. J. Sci. **17**, 961 (1934).

[38] H. Watanabe, Prog. Theor. Phys. **18**, 405 (1957).

[39] C. Hutchison, B. Judd, and D. Pope, Proc. Phys. Soc. London, Sect. B **70**, 514 (1957).

[40] S. A. Altshuler and B. M. Kozyrev, *Electron Paramagnetic Resonance of Compounds of Elements of Intermediate Groups* (Nauka, Moscow, 1972).

[41] B. Dai, T. Kato, S. Iwata, and S. Tsunashima, IEEE Trans. Magn. **48**, 3223 (2012).

[42] C. D. Stanciu, A. V. Kimel, F. Hansteen, A. Tsukamoto, A. Itoh, A. Kirilyuk, and T. Rasing, Phys. Rev. B **73**, 220402(R) (2006).

[43] J. Hohlfeld, T. Gerrits, M. Bilderbeek, T. Rasing, H. Awano, and N. Ohta, Phys. Rev. B **65**, 012413 (2001).

[44] J. Hohlfeld, C. D. Stanciu, and A. Rebei, Appl. Phys. Lett. **94**, 152504 (2009).

[45] C. D. Stanciu, A. Tsukamoto, A. V. Kimel, F. Hansteen, A. Kirilyuk, A. Itoh, and T. Rasing, Phys. Rev. Lett. **99**, 217204 (2007).

[46] A. Abragam and B. Bleaney, *Electron Paramagnetic Resonance of Transition Ions* (Oxford University Press, Oxford, 2012).